scientific reports



OPEN

Effects of aging on the physicomechanical, antimicrobial, and cytotoxicity properties of flowable composite resin with strontium-modified phosphate-based glass

Seo-Hyun Kim^{1,2,4}, Hye-Bin Go^{1,4}, Myung-Jin Lee³ & Jae-Sung Kwon^{1,2⊠}

This study investigated whether the various beneficial properties of flowable composite resin could be maintained upon adding strontium-modified phosphate-based glass (Sr-PBG) as an antibacterial agent. The experimental composite resin groups contained 1, 3, 5, or 10 wt% Sr-PBG. The mechanical, depth of cure, ion release, color analysis, surface gloss, antibacterial, and biocompatibility properties of the experimental groups were compared to those of the control group (100% resin). All experiments were performed before and after thermocycling to investigate the effects of thermal aging. Data were analyzed using one-way analysis of variance and Tukey's tests (p < 0.05). All mechanical properties for the experimental groups (e.g., flexural strength, elastic modulus, and microhardness) were significantly lower than those of the control group (p < 0.05). For Sr-PBG concentrations ≤ 5 wt%, the mechanical parameters were within the acceptable ranges set by ISO standards. Significant color differences (ΔE_{00}) were observed between the control and experimental groups, with the 10 wt% Sr-PBG sample showing clinically unacceptable levels. The release of Sr, P, and Ca ions increased with the Sr-PBG content before thermocycling. After thermocycling, Sr and Ca release decreased, whereas P release increased sharply at concentrations above 5 wt%. Antibacterial tests confirmed that higher Sr-PBG concentrations resulted in superior antibacterial efficacy against S. mutans. The Sr-PBGcontaining composites were not cytotoxic to human cells. The findings suggest that 5 wt% Sr-PBG is the optimal concentration for improving the antibacterial properties of dental restorative materials without compromising their clinical performance.

Keywords Antimicrobial, Flowable composite resin, Phosphate-based glass, Strontium

Flowable composite resins have gained significant attention as dental restorative materials owing to their excellent handling properties and diverse applications¹. These materials have demonstrated efficacy in restorative and prosthodontic dentistry and have been used as cavity liners and pit and fissure sealants, thereby helping to prevent lesion progression and reducing the need for further or more extensive restorations². The low viscosity of flowable composites enables them to conform to cavity walls, reducing the formation of voids and enhancing marginal integrity. In addition, flowable composites are increasingly used by dental practitioners owing to their ability to penetrate small defects and fissures, making them ideal for minimally invasive procedures.

Despite their widespread clinical success, flowable composites have inherent limitations. Their high degree of polymerization shrinkage can result in marginal gaps and compromised bonding interfaces, and their surfaces demonstrate higher susceptibility to bacterial adhesion and plaque accumulation than natural tooth enamel and

¹Department and Research Institute of Dental Biomaterials and Bioengineering, Yonsei University College of Dentistry, 50-1 Yonsei-ro, Seodaemun-gu, Seoul 03722, Republic of Korea. ²BK21 FOUR Project, Yonsei University College of Dentistry, Seoul, Republic of Korea. ³Department of Dental Hygiene, Division of Health Science, Baekseok University, Cheonan, Republic of Korea. ⁴Seo-Hyun Kim and Hye-Bin Go contributed to the work equally and should be regarded as co-first authors. [⊠]email: jkwon@yuhs.ac

other restorative materials³. These limitations frequently lead to significant clinical complications, including secondary caries, restoration fractures, postoperative sensitivity, and esthetic deterioration, which ultimately compromise the long-term durability and success of dental restorations^{4, 5}. Clinical studies have reported that the failure rate of restorations using flowable composites is significantly influenced by secondary caries, leading to repeated retreatments⁶. These treatment failures not only reduce the long-term success of restorations but also impose a considerable economic burden on both patients and healthcare systems⁷.

Over the past decades, extensive research has been conducted to develop flowable composite resins with improved clinical performance to overcome these challenges⁸. Various strategies have been investigated to enhance the antimicrobial properties of composite resins, including incorporating antibacterial agents (such as fluoride and chlorhexidine) into the resin matrix, modifying resin monomers to introduce quaternary ammonium functionalities, and integrating metal-oxide particles or ions with antibacterial activity⁹⁻¹³. Although these modifications have shown promising initial results in laboratory studies, their effectiveness is often limited by the short-term nature of the antibacterial release profile. Most of these materials exhibit a burst release pattern, in which most of the antibacterial agent is released within the first few days or weeks, followed by a rapid decline in therapeutic efficacy^{14, 15}. This short-lived antimicrobial activity fails to provide the sustained protection necessary for the long-term prevention of caries.

Strontium has been widely studied for dental and orthopedic applications because of its dual role in promoting bone regeneration and providing antibacterial activity¹⁶. The ability of Sr to enhance the bioactivity of dental materials makes it an attractive additive for improving the mechanical performance and therapeutic functionality of restorative composites¹⁷. Recent advancements have resulted in the development of Sr-modified phosphate-based glass (Sr-PBG), which has notable benefits due to its specialized composition and structure. Unlike conventional antibacterial additives, Sr-PBG exhibits controlled dissolution behavior, allowing for a steady and prolonged release of ions. Therefore, Sr-PBG delivers prolonged antimicrobial protection while supporting mineralization processes in adjacent dental structures¹⁸. When integrated into resin composites, Sr-PBG provides a reservoir of bioactive ions, including strontium, calcium, and phosphate, which are gradually released into the surrounding environment. These unique characteristics underscore the potential of Sr-PBG as a multifunctional additive for dental restorative materials, thereby addressing critical challenges, such as secondary caries and poor long-term durability.

Previous studies on the development of flowable composite resins with antibacterial properties focused on the effects of adding antibacterial ions such as Sr ions. However, few studies have investigated the sustained antibacterial effects achieved by incorporating Sr-PBG into flowable composite resins^{18, 19}. The rapid or uneven release of Sr-PBG into the oral environment may reduce the sustainability of its antibacterial efficacy. This study aims to evaluate the effects of various concentrations of Sr-PBG on the flexural strength, elastic modulus, microhardness, depth of cure, ion release, color, gloss, antibacterial properties, and cytotoxicity of flowable composites, focusing on their aging effects studied using a thermocycling accelerated aging method²⁰. The null hypothesis is that 1) various contents of Sr-PBG incorporated into the flowable composite resin do not affect the depth of cure, or the mechanical, chemical, optical, antibacterial, and biological properties; and 2) there are no significant differences in the aforementioned properties between the samples before and after thermocycling.

Materials and methods Glass preparation

To prepare Sr-PBG powder, P_2O_5 (50 mol%), CaO (15 mol%), Na $_2$ O (20 mol%), and SrO (15 mol%) were mixed in a tubular shaker for 1 h. Batches of the raw materials were melted in an alumina crucible at 1,100 $^{\circ}$ C for 1 h, and then the molten glass was quenched to produce glass cullets. The glass cullets were fragmented in an alumina mortar and powdered under dry conditions using a planetary monomill (Pulverisette-7; Fritsch, Idar-Oberstein, Germany). The particle size of the Sr-PBG powder was analyzed using an alumina crucible particle size analyzer (Mastersizer 2000; Malvern Instruments, Worcestershire, UK). To analyze the shape and elemental composition of the powder, field-emission scanning electron microscopy (FE-SEM; JSM-7800 F, JEOL, Akishima, Tokyo, Japan) and energy-dispersive X-ray spectroscopy (EDS) were performed, respectively. The amorphous structure of Sr-PBG was confirmed using X-ray diffraction (XRD; Ultima IV, Rigaku, Tokyo, Japan).

Preparation of flowable composite resins containing Sr-PBG

A commercially available flowable composite resin (G-Aenial Universal Flo; GC, Tokyo, Japan) was used as the matrix material. The experimental groups were prepared by homogeneously mixing various weight percentages of Sr-PBG powder into the resin by manual mixing. The experimental groups are henceforth called 1 wt%, 3 wt%, 5 wt%, and 10 wt% corresponding to the Sr-PBG contents, with the remainder comprising the flowable composite resin. The original composite resin without Sr-PBG powder was used as the control group. After mixing, the specimens were cured using a light-curing unit (Elipar DeepCure-L 76973; 3M ESPE Co., Seefeld, Germany) (Table 1). Accordingly, these five groups were as below:

Flexural strength and elastic modulus

The flexural strength and elastic modulus of the flowable composite resins were measured following ISO 4049 standards. Seven specimens, each with a length of 25 mm, width of 2 mm, and height of 2 mm, were fabricated for each experimental and control group. Each resin specimen was light-cured on both sides according to the ISO-specified method, using five slightly overlapping irradiation regions for 20 s each. Specimens containing air bubbles or voids were excluded from analysis. A thermocycling system (Thermal Cyclic Tester; R&B Inc., Daejeon, Korea) was used to treat the samples using 45 s dips (with a 5 s transfer time) in distilled water between 5 and 55 °C for 850 cycles, corresponding to a duration of 1 month. The as-prepared specimens (without

Groups	Flowable composite resin content (wt%)	Sr-PBG content (wt%)
Control	100	0
1 wt%	99	1
3 wt%	97	3
5 wt%	95	5
10 wt%	90	10

Table 1. Composition of flowable composite resin formulations.

thermocycling) were stored at 37 $^{\circ}$ C in distilled water for 24 h before testing, while the specimens subjected to thermocycling were tested immediately.

Three-point bending fracture tests were performed using a universal testing machine (Model 5942; Instron, MA, USA). The test conditions included a span length (l) of 20 mm and crosshead speed of 1 mm/min. The flexural strength, σ , and elastic modulus, E, were calculated using Eqs. (1) and (2), respectively.

$$\sigma = \frac{3Fl}{2bh^2} \tag{1}$$

$$E = \frac{Pl^3}{4bh^3d} \tag{2}$$

Here, F is the maximum load exerted on the specimen (N), b is the specimen width (mm), h is the specimen height (mm) measured immediately before the test, P is the load at a point on the linear region of the load–displacement curve (N), and d is the deflection at load P (mm).

Microhardness

Vickers microhardness values were determined using five disc-shaped specimens for each group, each with a diameter of 10 mm and a height of 2 mm. Prior to testing, specimens were subjected to thermocycling treatment using a thermocycling system (Thermal Cyclic Tester; R&B Inc., Daejeon, Korea) with 45 s dips (with a 5 s transfer time) into distilled water between 5 and 55 °C for 850 cycles, corresponding to a duration of 1 month. A microhardness tester (MMT-X7B; Matsuzawa Seiki Co., Tokyo, Japan) fit with a Vickers diamond indenter was used. During testing, a 300 g load was applied for 15 s. Three sites were randomly measured for each specimen and the mean values and standard deviations were obtained and compared for all experimental and control groups.

Depth of cure

The specimens for the depth of cure experiments were prepared following ISO 4049 standards. Specimens from each group (n = 5) were prepared using cylindrical polytetrafluoroethylene (PTFE) molds (6 mm in length and 4 mm in diameter). The specimens were vertically cured for 20 s using a light-curing unit (Elipar DeepCure-L 76973; 3M ESPE Co., Seefeld, Germany). After polymerization, the unpolymerized material at the bottom of the specimen was gently removed using a plastic spatula. The height of the produced specimens was measured with a digital Vernier caliper (CD-15APX; Mitutoyo Co., Kanagawa Prefecture, Japan) with an accuracy of \pm 0.1 mm. The longest and shortest dimensions were measured twice and the values were averaged and recorded.

Ion release

To observe the ion release from the composites, each specimen was prepared using a metal mold with a diameter of 10 mm and a height of 2 mm. Ion release was evaluated both before and after thermocycling. A thermocycling system (Thermal Cyclic Tester; R&B Inc., Daejeon, Korea) was used to treat the samples using 45 s dips (with a 5 s transfer time) in distilled water between 5 and 55 °C for 850 cycles, corresponding to a duration of 1 month. Specimens from each group (n=5) were placed in 5 mL of distilled water and stored in a shaking incubator at 37 °C. To measure the initial ion release rate, the eluted ions were collected after incubation for 24 h and the abundance of each ion was measured. Elemental analyses of Sr, P, and Ca ions were performed using an inductively coupled plasma optical emission spectrometer (Agilent 5110; Agilent, CA, USA).

Color analysis

Specimens (n = 3 for each group) were prepared using cylindrical molds with a diameter and height of 10 and 2 mm, respectively. The surfaces of the cured samples were polished sequentially using carbide paper of 800 and 1000 grit sizes using a polishing machine (EcoMet 30; Buehler, IL, USA). The color of the specimens was measured both before and after thermocycling according to the CIE $L^*a^*b^*$ color scale, relative to the standard illuminant D65, using a spectrophotometer (CM-5; Konica Minolta, Osaka, Japan)²¹. A thermocycling system (Thermal Cyclic Tester; R&B Inc., Daejeon, Korea) was used to treat the samples using 45 s dips (with a 5 s transfer time) in distilled water between 5 and 55 °C for 850 cycles, corresponding to a duration of 1 month. In the CIE $L^*a^*b^*$ system, the specific shaded position of the color space is defined using three coordinates: L^* represents the lightness of the color and ranges between 0 (dark) and 100 (light); a^* represents a color on the red (positive)–green (negative) axis; and b^* represents a color on the yellow (positive)–blue (negative) axis. The

measurements were repeated three times for each specimen. Additionally, the color difference was calculated using the CIEDE2000 formula, as shown in Eq. (3).

$$\Delta E_{00} = \sqrt{\left(\frac{\Delta L'}{K_L S_L}\right)^2 + \left(\frac{\Delta C'}{K_C S_C}\right)^2 + \left(\frac{\Delta H'}{K_H S_H}\right)^2 + R_T \left(\frac{\Delta C'}{K_C S_C}\right) \left(\frac{\Delta H'}{K_H S_H}\right)}$$
(3)

Here, ΔE_{00} represents the color difference, where L (Value) indicates the degree of lightness, C (Chroma) refers to the degree of saturation, and H (Hue) denotes the color tone. The scale factors S_L , S_C and S_H are applied to correct the differences in lightness, chroma, and hue, respectively. The parametric factors K_L , K_C and K_H are correction parameters for K_L , K_C and K_H respectively, and were set to 1.

Surface gloss

The surface gloss of the specimens was measured using a gloss meter (Novo-Curve; Rhopoint Instrumentation, East Sussex, UK). Gloss measurements were conducted both before and after thermocycling. A thermocycling system (Thermal Cyclic Tester; R&B Inc., Daejeon, Korea) was used to treat the samples by alternately immersing them in distilled water at 5 °C and 55 °C for 45 s each (with a 5 s transfer time) for a total of 850 cycles, simulating approximately 1 month of clinical use. The specimens were fabricated using metal molds with a thickness of 2 mm and diameter of 10 mm. The cured specimens were mounted on the gloss meter for measurements. Measurements were performed on five specimens from each group, and three points were randomly selected for each specimen. The flat surfaces were measured using a 60° geometry.

Antibacterial properties

Disc-shaped specimens for each group were prepared using a mold with a diameter of 10 mm and a height of 2 mm. Antibacterial tests were performed both before and after thermocycling. A thermocycling system (Thermal Cyclic Tester; R&B Inc., Daejeon, Korea) was used to alternately immerse the samples in distilled water at 5 °C and 55 °C for 45 s each (with a 5 s transfer time) for a total of 850 cycles, simulating approximately 1 month of clinical use. The bacterial strain used in the experiments was *Streptococcus mutans* (*S. mutans*, ATCC 25175). *S. mutans* was cultured in Brain Heart Infusion broth at 37 °C for 24 h. The optical density (OD) at 600 nm was adjusted to 0.04, and the diluted bacterial suspension was placed directly on the composite disc samples (n = 15). The bacterial solution applied onto the disc was removed, and 1 mL of solution was dropped onto BHI solid medium, spread, and incubated at 37 °C for 24 h. After incubation, the number of colony-forming units (CFU) was counted and the average values and standard deviations were calculated.

Cytotoxicity

Cell viability was assessed using L929 cells (ATCC, CCL-1, American type culture collection, San Diego, CA, USA), and the WST-1 assay was used to quantify the cleavage of WST-1 (4-[3-(4-iodophenyl)-2-(4-nitro-phenyl)-2H-5-tetrazolio]-1,3-benzene sulfonate) by mitochondrial dehydrogenases. Cells were seeded in 96-well culture plates at a density of 1×10^5 cells/well and allowed to adhere for 24 h at 37 °C in a 5% CO $_2$ atmosphere. After this period, the culture medium was removed, and 100 μL of the extracts from each group were added to all wells containing the attached cells. After further incubation in a humidified CO $_2$ incubator at 37 °C for 24 h, 10 μL of WST-1 reagent was added, and the cells were incubated for an additional 2 h before reading the OD. Absorbance was measured at 450 nm using a microplate spectrophotometer (Epoch, BioTek; VT, USA). Cell viability was calculated as the percentage of the OD of the test group compared to that of the negative control. The cell viability was evaluated according to the ISO 10993-5 standard.

Statistical analysis

All statistical analyses were conducted using IBS SPSS software (version 25.0; IBM Korea Inc., Seoul, Korea) with data obtained from independent experiments. Prior to conducting the one-way ANOVA, the normality of data distributions was confirmed using the Shapiro–Wilk test (p > 0.05). The results obtained for both control and experimental groups were subjected to one-way analysis of variance (ANOVA), followed by Tukey's post-hoc tests. In all analyses, the level of statistical significance was set at p < 0.05.

In this study, the number of specimens per group was determined by reference to previous studies on flowable dental composites, which typically employ comparable sample sizes to achieve a statistical power of approximately 80% with a significance level of 0.05. This sample size was considered sufficient to detect clinically relevant differences based on effect sizes reported in the literature.

Results

Characterization of Sr-PBG powder

Figure 1 presents the characterization results for the Sr-PBG powder. The XRD pattern of the Sr-PBG powder (Fig. 1A) shows the absence of sharp peaks, consistent with the amorphous structure of typical glass materials. The particle-size distribution of the Sr-PBG powder (Fig. 1B) exhibits a bimodal distribution, with distribution intensity peaks at 1.92 and 56.92 μ m. The FE-SEM/EDS images of the Sr-PBG powder in Fig. 1C show the particle morphology and verify the homogeneous distribution of O, P, Ca, Sr, and Na within the material.

Flexural strength and elastic modulus

Figure 2 shows the effect of thermocycling on the mechanical properties (flexural strength and elastic modulus) of the composite resin samples. Before and after thermocycling, the control group consistently exhibits the highest flexural strength (Fig. 2A, B, respectively), and the strength significantly decreases with increasing Sr-

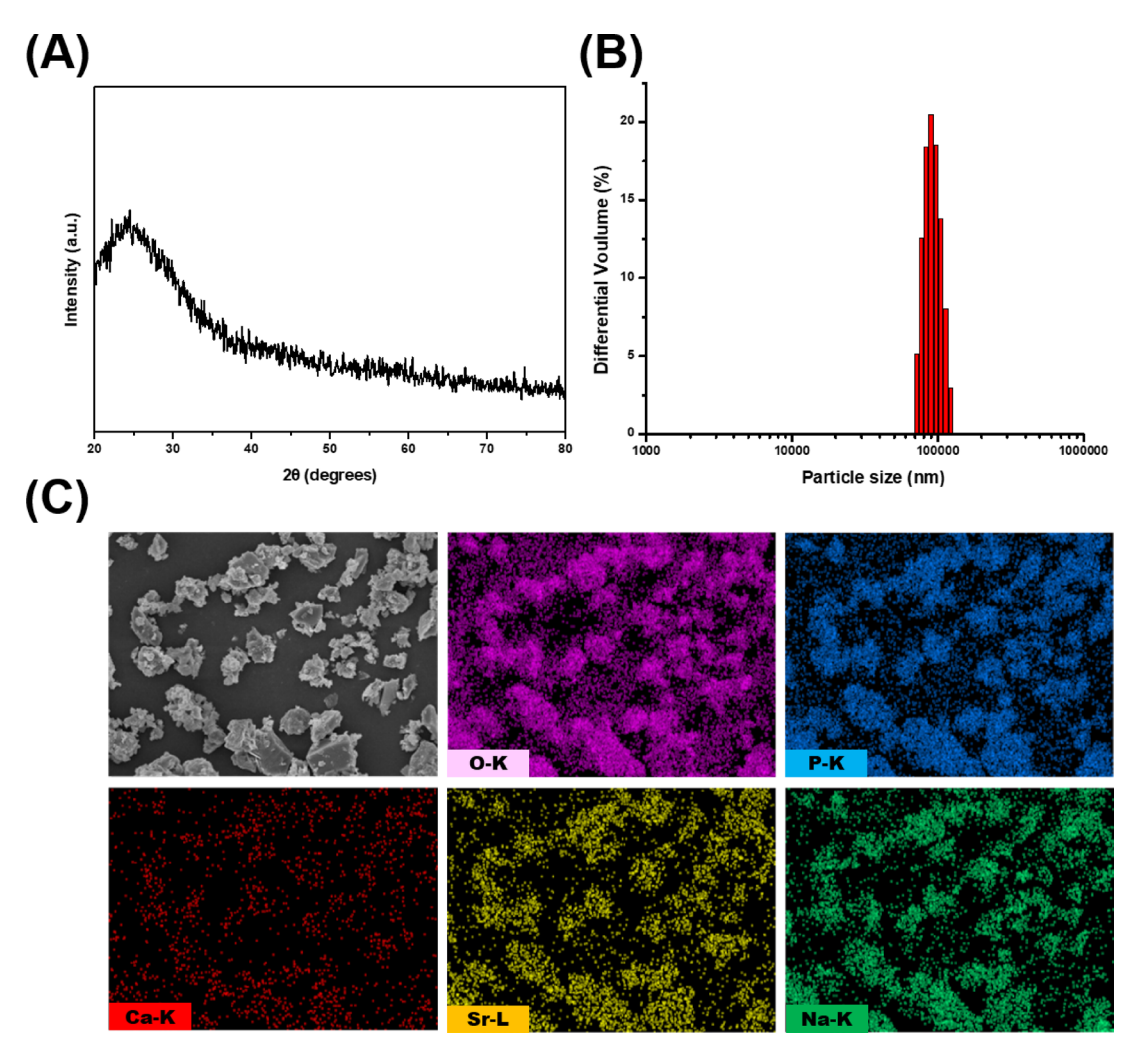


Fig. 1. Characterization of Sr-PBG powder. **(A)** XRD pattern, **(B)** particle size distributions, and **(C)** FE-SEM image of Sr-PBG powder with overlapping EDS maps of the distributions of selected elements. EDS, energy dispersive X-ray spectroscopy; FE-SEM, field-emission scanning electron microscopy; Sr-PBG, strontium-modified phosphate-based glass; XRD, X-ray diffraction.

PBG content (p<0.05). Figure 2C shows a significant difference in the elastic moduli between the control group and experimental groups before thermocycling (p<0.05). The moduli for the 1, 3, and 5 wt% groups are notably higher than that of the control group, whereas the 10 wt% group exhibits no significant difference. However, after thermocycling (Fig. 2D), the 5 and 10 wt% groups show significantly lower values than the control group (p<0.05).

Microhardness

The microhardness values before and after thermocycling are shown in Fig. 2C, F, respectively. The control group exhibits the highest microhardness before and after thermocycling, and these values are significantly different from those for the experimental groups. In particular, after thermocycling (Fig. 2F), the 1 wt% group shows no significant difference in microhardness compared to the control group. However, the microhardness gradually decreases with increasing Sr-PBG content.

Depth of cure

Figure 3 compares the depths of cure measured for the control and experimental groups. The control group exhibits the lowest value of 5.88 ± 0.06 mm, while the 1, 3, 5, and 10 wt% experimental groups exhibit values of 5.93 ± 0.03 mm, 5.98 ± 0.01 mm, 5.98 ± 0.04 mm, and 5.94 ± 0.03 mm, respectively. No significant differences are observed between experimental groups. According to ISO 4049, the depth of cure must be at least 1.5 mm.

Ion release

Figure 4 shows the amount of Sr, P, and Ca ions released before and after thermocycling. Before thermocycling (Fig. 4A), the detected Sr content in the control group is very low (~0.1 ppm). However, the Sr, P, and Ca contents increase with increasing Sr-PBG content. When the Sr-PBG content exceeded 5 wt%, the concentrations of Sr, P,

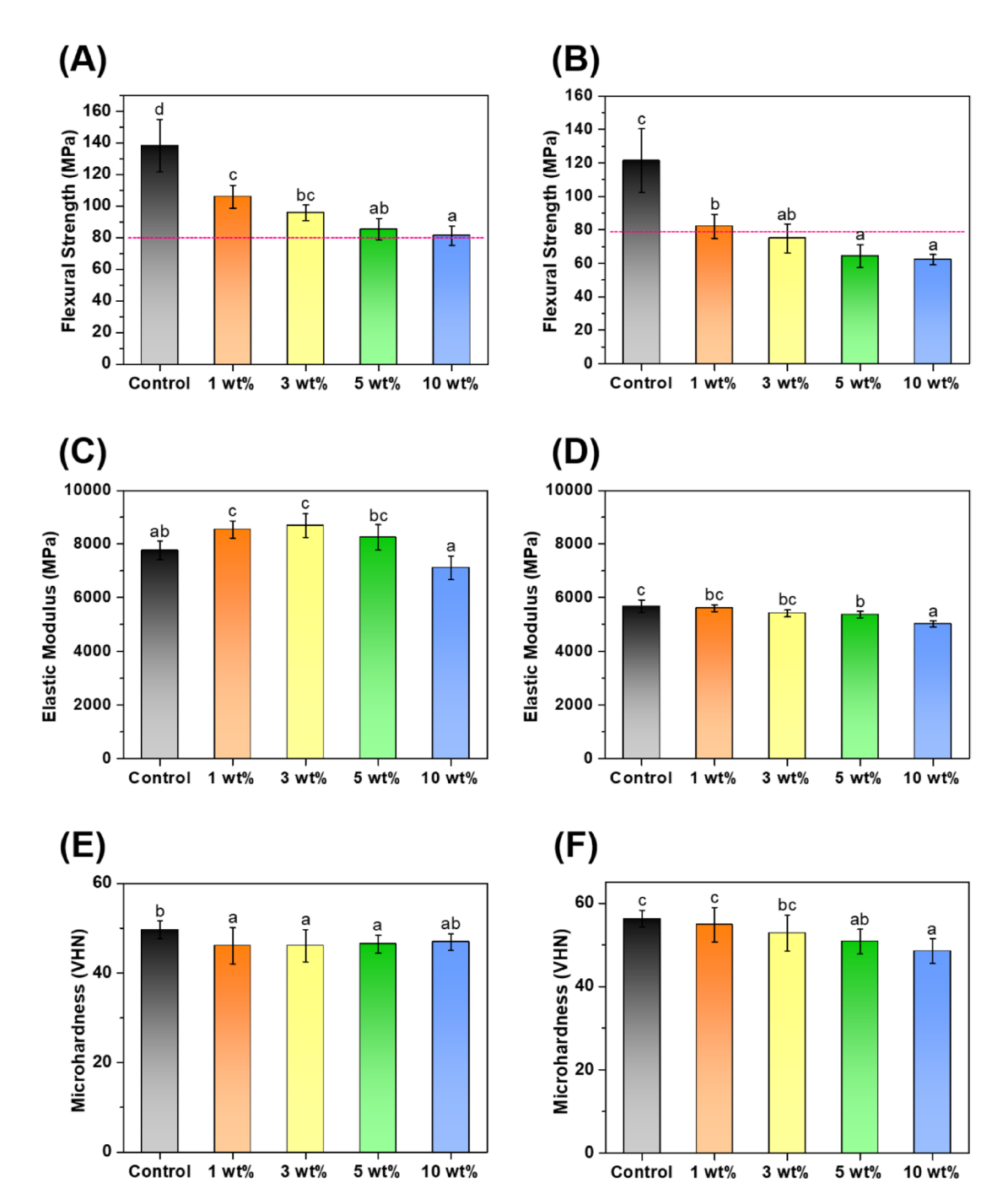


Fig. 2. Mechanical properties of flowable composite resins containing strontium-modified phosphate-based glass, with clear differences observed before (A, C, E) and after (B, D, F) thermocycling for testing; (A, B) Flexural strength, (C, D) elastic modulus, and (E, F) Vickers microhardness. Different lowercase letters above the error bars indicate significant differences, as determined by the Tukey's post-hoc test. Error bars represent the standard deviation of the mean.

and Ca sharply increased. At 5 wt%, Sr and P were both approximately 51 ppm, and Ca was 24 ppm. At 10 wt%, Sr and P reached 110 ppm, while Ca increased to 53 ppm. Compared to the data obtained before thermocycling, similar results are observed after thermocycling (Fig. 4B), but fewer Sr and Ca ions are released. However, the release of P ions increases sharply for ≥ 5 wt% Sr-PBG.

Color values

Table 2 summarizes the L^* , a^* , and b^* values in comparison to the control group, while Table 3 presents the color values of the control and experimental groups before and after thermocycling. The control group exhibits the lowest lightness (L^*) and redness–greenness (a^*) values, which significantly increase with increasing Sr-

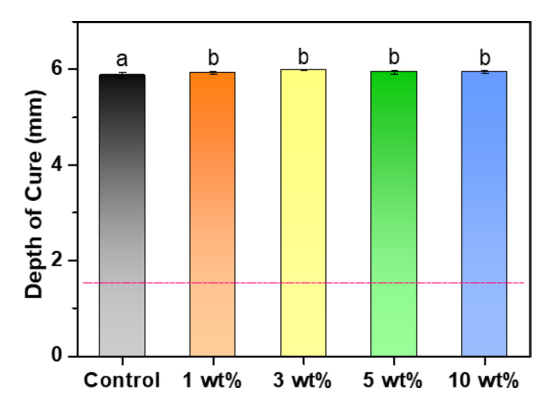


Fig. 3. Depths of cure for the control and experimental groups. Different letters indicate significant differences at p < 0.05.

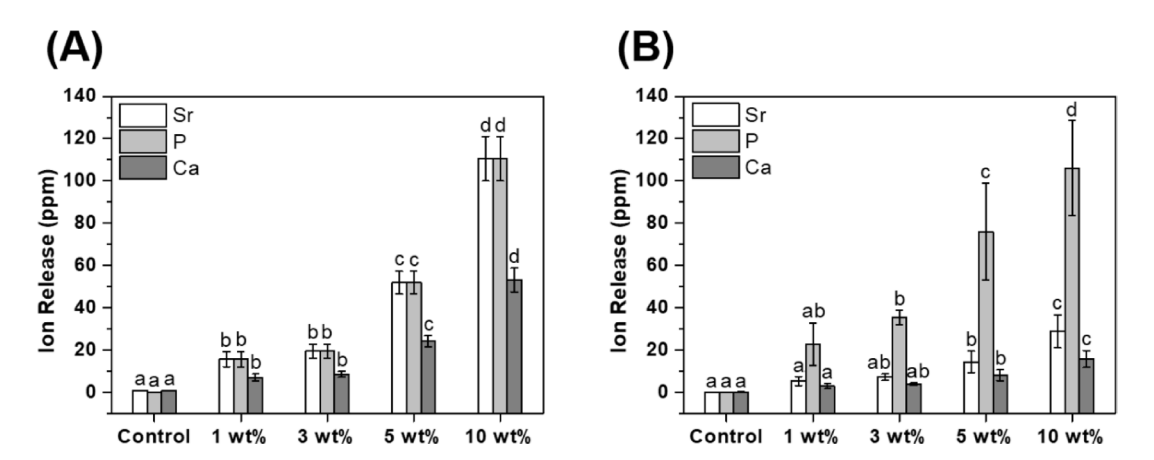


Fig. 4. Concentrations of the Sr, P, and Ca ions released from each group: (**A**) before and (**B**) after thermocycling. Error bars represent the standard deviations of the means. Different lowercase letters above the error bars indicate significant differences between the elements (Sr, P, and Ca), as determined by the Tukey's post-hoc test.

Thermocycling	Groups	L*	a*	b*
	Control	70.46 ± 0.60 a	0.77 ± 0.12^a	9.83 ± 0.44^{a}
	1 wt%	72.08 ± 0.46^{b}	0.81 ± 0.04^{a}	10.31 ± 0.42 bc
Before	3 wt%	73.67 ± 0.49°	0.93 ± 0.05^{b}	10.23 ± 0.27 abc
	5 wt%	75.52 ± 0.35^{d}	1.06 ± 0.07^{c}	10.50 ± 0.23°
	10 wt%	78.56 ± 0.59e	1.08 ± 0.09^{c}	9.86 ± 0.32^{ab}
	Control	68.20 ± 0.22^a	1.04 ± 0.04^a	12.63 ± 0.19 ^a
	1 wt%	69.75 ± 0.44 ^b	1.09 ± 0.04^{a}	11.82 ± 0.21^{ab}
After	3 wt%	72.08 ± 0.33°	1.09 ± 0.03^a	11.82 ± 0.23^{ab}
	5 wt%	73.19 ± 0.37^{d}	1.19 ± 0.05^{b}	11.96 ± 0.26 ^b
	10 wt%	75.89 ± 0.27^{e}	1.27 ± 0.06^{c}	11.54 ± 0.20 ^a

Table 2. Color values of the control group and experimental groups before and after thermocycling.

PBG content (p<0.05). The thermocycled control group shows the highest blueness–yellowness (b^*) values, which increase with increasing Sr-PBG content and then decrease at 10 wt% Sr-PBG. Information regarding the color differences measured using CIEDE2000 is presented in Table 2. According to recent studies, $\Delta E_{00} \le 1.7$ is considered imperceptible, $1.7 < \Delta E_{00} \le 4.1$ is considered perceptible, and $\Delta E_{00} > 4.1$ is considered unacceptable²².

The same lowercase letter in the same column indicates no significant difference (p > 0.05).

The same letter in the same column indicate no significant difference (p > 0.05).

Groups	Before thermocycling ΔE_{00}	After thermocycling ΔE_{00}	ΔE_{00} (Before-After)
Control	_	_	2.63 ± 0.30 ^c
1 wt%	1.35 ± 0.38 ^a	1.35 ± 0.34 ^a	2.10 ± 0.19^{ab}
3 wt%	2.48 ± 0.81 ^b	3.06 ± 0.35 ^b	1.64 ± 0.32 ^a
5 wt%	3.60 ± 0.73°	3.86 ± 0.39°	1.99 ± 0.44^{ab}
10 wt%	5.98 ± 0.43 ^d	5.86 ± 0.21 ^d	2.24 ± 0.43 ^{bc}

Table 3. Comparison of the control group and experimental groups and difference in ΔE_{00} values based on the presence or absence of thermocycling.

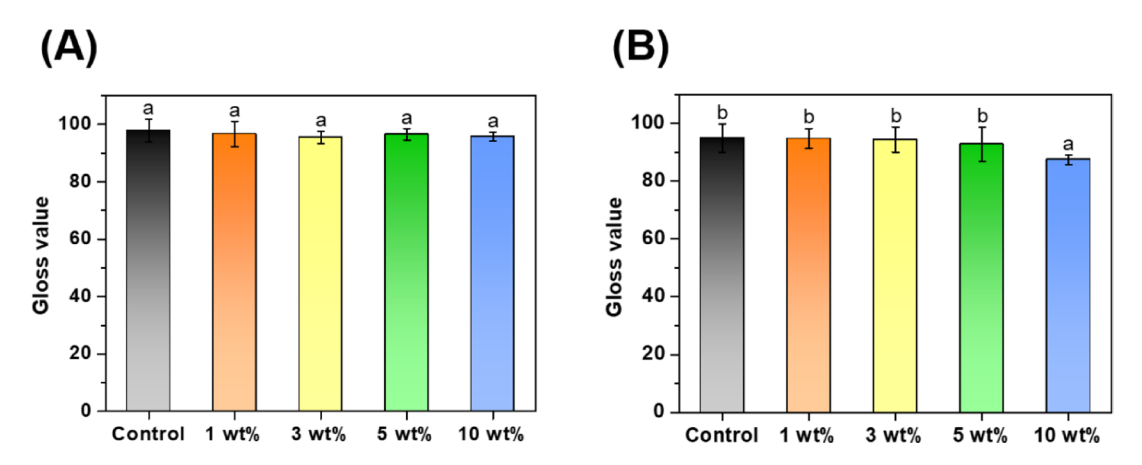


Fig. 5. Comparison of the gloss values of strontium-modified flowable composites (**A**) before and (**B**) after thermocycling. Different letters indicate significant differences at p < 0.05.

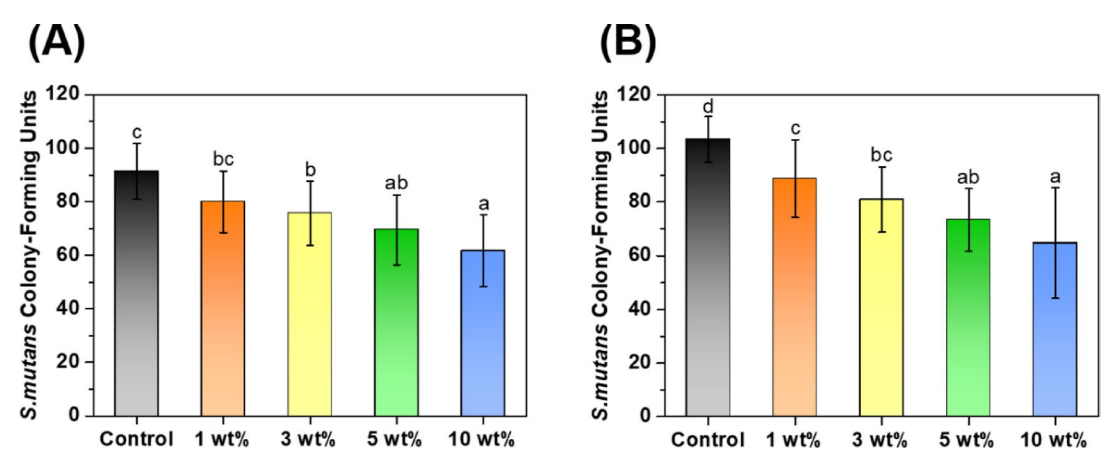


Fig. 6. Comparison of CFU counts for *S. mutans* on the sample surfaces: (**A**) before and (**B**) after thermocycling.

Gloss Values

Figure 5 compares the gloss values of the flowable composite specimens with increasing Sr-PBG content. No significant differences are observed between any of the groups before thermocycling (Fig. 5A). However, in the post-thermocycling groups (Fig. 5B), significant differences are observed only for the 10 wt% Sr-PBG group.

Antibacterial Properties

Figure 6 compares the CFU counts of *S. mutans* on the sample surfaces. All experimental groups show a significant difference compared with the control group (p < 0.05). The inclusion of Sr-PBG inhibits *S. mutans* regardless of thermocycling.

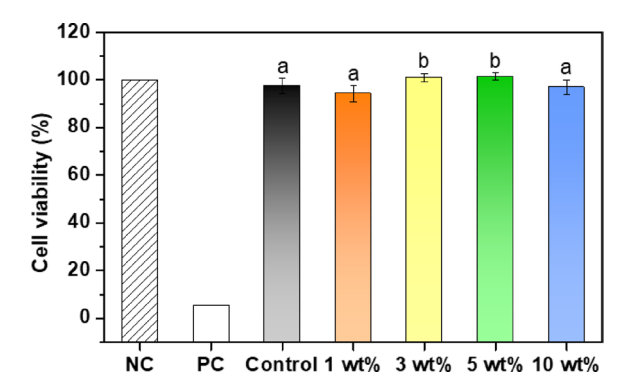


Fig. 7. Cell viability of control and experimental groups. Different lowercase letters indicate significant differences at p < 0.05. NC, negative control; PC, positive control.

Cytotoxicity

Figure 7 evaluates the viability of L929 cells. There are no significant differences between the 1 and 10 wt% Sr-PBG groups compared with the control group, but significant differences are observed for the 3 and 5 wt% Sr-PBG groups. The cell viabilities are $97.39 \pm 3.19\%$ for the control group, and $94.22 \pm 3.50\%$, $100.90 \pm 1.65\%$, $101.28 \pm 1.53\%$, and $96.89 \pm 3.00\%$ for the 1, 3, 5, and 10 wt% Sr-PBG groups, respectively.

Discussion

Flowable composite resins present significant advantages in dental applications because of their excellent handling properties. However, their susceptibility to bacterial colonization and secondary caries formation remains a substantial clinical challenge^{23, 24}. This study investigated the incorporation of Sr-PBG into a flowable composite resin to develop a composite material with sustained antibacterial properties that maintains the essential physicomechanical characteristics of the original resin.

The oral environment is constantly exposed to humid conditions, making it clinically important to understand how these conditions affect the material properties²⁵. In particular, several studies have reported that thermocycling over a temperature range of 5–55 °C can simulate the aging process in clinical settings^{20, 26}. In this study, thermocycling (850 cycles between 5 and 55 °C) was used to simulate approximately one month of clinical use^{18, 27}. The observed reduction in flexural strength of the control flowable composite from 138 ± 16 to 121 ± 19 MPa after this thermocycling process is consistent with the results of previous studies demonstrating the deteriorative effects of thermal stress on composite materials^{26, 28}.

A novel aspect of this study is the demonstration of sustained antibacterial activity and preserved depth of cure in flowable composites containing up to 5 wt% Sr-PBG, even after thermocycling. Unlike conventional antibacterial fillers, which typically exhibit a short-term burst release, Sr-PBG showed controlled ion release with retained antimicrobial effects under aging conditions. This finding aligns with previous work on strontium-based glass fillers but extends their application to flowable composites, which have not been widely explored $^{15-17}$. Furthemore, the XRD pattern showing the absence of sharp diffraction peaks confirmed the amorphous nature of the synthesized Sr-PBG 29 . This non-crystalline structure is a hallmark of glassy materials and is favorable for sustained ion release, which is beneficial in the context of bioactive dental materials 29 . The bimodal particle distribution (peaks at 1.81 and 49.66 μ m) and homogeneous elemental dispersion demonstrated by EDS indicate the successful synthesis of Sr-PBG with appropriate physical characteristics for incorporation into dental materials $^{19,\,30}$.

Analysis of the mechanical properties revealed a concentration-dependent relationship between the Sr-PBG content and flexural strength. The significant decrease in strength with increasing Sr-PBG concentration is attributed to stress concentration points at the interface between the glass particles and resin matrix³⁰. However, it is noteworthy that specimens containing up to 5 wt% Sr-PBG maintained flexural strength values above the minimum requirements specified by ISO 4049 for restorative materials. This suggests that a limited incorporation of Sr-PBG maintains the mechanical integrity of the resin for clinical applications. Similar trends were observed in the elastic modulus and microhardness data. Before thermocycling, the experimental groups with 1–5 wt% Sr-PBG exhibited higher elastic moduli than the control group, potentially owing to the reinforcing effect of well-dispersed glass particles at lower concentrations. However, after thermocycling, a concentration-dependent decrease in the elastic moduli was observed, with the 5 and 10 wt% groups exhibiting significantly lower values. This suggests that thermal stress may degrade the interface between the Sr-PBG particles and the resin matrix, particularly at higher filler concentrations.

The depth-of-cure data are particularly noteworthy, as all experimental groups demonstrated adequate polymerization depths that exceeded the ISO requirements. The depth of cure is assessed to ensure that no uncured material remains, which could lead to clinical problems. Although FT-IR spectroscopy allows for the quantitative analysis of polymerization and material reactions, it requires the specimen to be pulverized. Therefore, in this study, the depth of cure was evaluated using the method described in ISO 4049³¹.

The incorporation of Sr-PBG resulted in increased lightness (L^*), which is attributed to the inherent white color of the glass particles. The color difference (ΔE_{00}) between the control and experimental groups increased

proportionally with Sr-PBG concentration, exceeding the clinically acceptable threshold at 10 wt% 22 . This finding has important clinical implications, particularly for anterior restorations where esthetic considerations are paramount, suggesting that the Sr-PBG content should be limited to ≤ 5 wt% to maintain acceptable color matching.

The ion-release data provide valuable insights into the bioactive potential of the studied materials. Before thermocycling, Sr, P, and Ca release was concentration dependent, with markedly higher release rates at ≥ 5 wt% Sr-PBG. The post-thermocycling evaluation revealed an interesting shift in the release patterns compared to the materials before thermocycling; the rates of Sr and Ca release are lower but P release is substantially higher at higher Sr-PBG concentrations. This changes in the release profile after aging indicate dynamic changes in the surface chemistry and dissolution behavior of the material, which may affect long-term antibacterial efficacy and remineralization capacity.

The antibacterial efficacy of the experimental materials against *S. mutans* was confirmed by the significant reduction in CFU counts with increasing Sr-PBG content. The persistence of this effect after thermocycling suggests sustained antibacterial activity under simulated clinical conditions^{18, 32}. This is attributed to the continuous release of Sr ions (as evidenced by the ion-release data) and represents a significant advantage over conventional antibacterial additives, which typically exhibit burst-release profiles³³.

Cell viability evaluations confirmed the biocompatibility of the Sr-PBG-containing materials, with all experimental groups maintaining cell viability above 90%. The slightly higher cell viability for the 3 and 5 wt% Sr-PBG groups compared with the control warrants further investigation into the potential bioactive effects of moderate Sr-PBG concentrations on cellular responses 16.

Based on the results, the first null hypothesis—that incorporating Sr-PBG into flowable composite resin does not affect its mechanical, chemical, optical, antibacterial, and biological properties—was partially rejected. While depth of cure and cytotoxicity remained unaffected (p > 0.05), significant changes were observed in flexural strength, ion release, color stability, and antibacterial activity depending on Sr-PBG concentration (p < 0.05). The second null hypothesis—that thermocycling does not affect these properties—was also partially rejected, as thermocycling led to declines in mechanical properties and changes in ion release and color values, although depth of cure, antibacterial effect, and cell viability were maintained. These findings suggest that up to 5 wt% Sr-PBG offers a balance between enhanced antibacterial function and acceptable physical performance.

Although this study provides comprehensive data on the physicomechanical, antibacterial, and biological properties of Sr-PBG containing flowable composites, certain limitations should be acknowledged. The in vitro experiments do not fully replicate the complex oral environment; for example, this study focused on a single bacterial species, whereas the oral cavity harbors a diverse microbiome. Additionally, the thermocycling protocol, while standardized, represents only approximately one month of clinical service. Future research should include long-term aging studies, multispecies biofilm models, and clinical trials to validate these promising results.

Conclusions

In conclusion, the incorporation of 5 wt% Sr-PBG into a flowable composite resin appears to be a promising strategy for enhancing antibacterial properties without compromising the physicomechanical and optical characteristics of the material. The experimental resin exhibited acceptable flexural strength, elastic modulus, and microhardness, along with sustained antibacterial activity against *S. mutans*. Additionally, the release of Sr, Ca, and P ions may contribute to both bacterial resistance and potential remineralization. These findings suggest that Sr-PBG is a viable additive for developing advanced dental restorative materials; however, further long-term in vivo studies are necessary to confirm these benefits and assess clinical durability.

Data availability

The datasets generated and/or analysed during the current study are available from the corresponding author upon reasonable request.

Received: 16 May 2025; Accepted: 23 July 2025

Published online: 04 August 2025

References

- 1. Shrestha, B., Aati, S., Maria Rajan, S. & Fawzy, A. Flowable resin-based composites modified with chlorhexidine-loaded mesoporous silica nanoparticles induce superior antibiofilm properties. *J. Nanopart. Res.* 26, 140 (2024).
- 2. Zhou, X. et al. Development and status of resin composite as dental restorative materials. J. Appl. Polym. Sci. 136, 48180 (2019).
- 3. Lee, M.-J. et al. Development of a bioactive flowable resin composite containing a zinc-doped phosphate-based glass. *Nanomaterials* **10**, 2311 (2020).
- 4. van Dijken, J. W. & Pallesen, U. A six-year prospective randomized study of a nano-hybrid and a conventional hybrid resin composite in Class II restorations. *Dent. Mater.* 29, 191–198 (2013).
- 5. Kopperud, S. E., Tveit, A. B., Gaarden, T., Sandvik, L. & Espelid, I. Longevity of posterior dental restorations and reasons for failure. Eur. J. Oral. Sci. 120, 539–548 (2012).
- 6. Baroudi, K. et al. Flowable resin composites: A systematic review and clinical considerations. *J. Clin. Diagn. Res.* **9**(6), ZE18–ZE24 (2015).
- 7. Demarco, F. F. et al. Should my composite restorations last forever? Why are they failing?. Braz. Oral Res. 56, 28–31 (2017).
- 8. van de Sande, F. H. et al. The influence of different restorative materials on secondary caries development in situ. *J. Dent.* 42, 1171–1177 (2014).
- Yao, S. et al. Novel antibacterial and therapeutic dental polymeric composites with the capability to self-heal cracks and regain mechanical properties. Eur. Polym. J. 129, 109604 (2020).
- Hojati, S. T. et al. Antibacterial, physical and mechanical properties of flowable resin composites containing zinc oxide nanoparticles. Dent. Mater. 29, 495–505 (2013).
- 11. Leung, D. et al. Chlorhexidine-releasing methacrylate dental composite materials. Biomaterials 26, 7145-7153 (2005).

- 12. Weng, Y., Guo, X., Gregory, R. L. & Xie, D. Preparation and evaluation of an antibacterial dental cement containing quaternary ammonium salts. J. Appl. Sci. 122, 2542–2551 (2011).
- Cheng, L. et al. Effect of amorphous calcium phosphate and silver nanocomposites on dental plaque microcosm biofilms. J. Biomed. Mater. Res. B. Appl. Biomater. 100, 1378–1386 (2012).
- Souza, L. V. S. et al. Mechanical and antibacterial properties of an experimental flowable composite containing Nb₂O₅ and NF_TiO, nanoparticles. J. Mech. Behav. Biomed. Mater. 143, 105919 (2023).
- 15. Chen, L., Suh, B. I. & Yang, J. Antibacterial dental restorative materials: A review. Am J Dent. 31, 6b-12b (2018).
- 16. Jayasree, R. et al. Dentin remineralizing ability and enhanced antibacterial activity of strontium and hydroxyl ion co-releasing radiopaque hydroxyapatite cement. J. Mater. Sci. Mater. Med. 28, 95 (2017).
- 17. Nielsen, S. P. The biological role of strontium. Bone 35, 583-588 (2004).
- 18. Go, H.-B., Lee, M.-J., Seo, J.-Y., Byun, S.-Y. & Kwon, J.-S. Mechanical properties and sustainable bacterial resistance effect of strontium-modified phosphate-based glass microfiller in dental composite resins. Sci. Rep. 13, 17763 (2023).
- 19. Jang, E.-J. et al. In vitro antifungal and physicochemical properties of polymerized acrylic resin containing strontium-modified phosphate-based glass. *BMC Oral Health* 24, 775 (2024).
- 20. Ghavami-Lahiji, M. et al. The effect of thermocycling on the degree of conversion and mechanical properties of a microhybrid dental resin composite. *Restor. Dent. Endod.* 43, e26 (2018).
- 21. CIE, C. Bureau Central de la CIE (1986).
- Coelho, S. R. et al. Effect of immersion in disinfectants on the color stability of denture base resins and artificial teeth obtained by 3D printing. J. Prosthodont. 33, 157–163 (2024).
- 23. Vouvoudi, E. C. Overviews on the progress of flowable dental polymeric composites: Their composition, polymerization process, flowability and radiopacity aspects. *Polymers* 14, 4182 (2022).
- 24. Kattan, H. et al. Physical properties of an Ag-doped bioactive flowable composite resin. Materials 8, 4668-4678 (2015).
- 25. Janda, R., Roulet, J.-F. & Latta, M. The effects of thermocycling on the flexural strength and flexural modulus of modern resinbased filling materials. *Dent. Mater.* 22, 1103–1108 (2006).
- 26. Kiomarsi, N., Saburian, P., Chiniforush, N., Karazifard, M.-J. & Hashemikamangar, S.-S. Effect of thermocycling and surface treatment on repair bond strength of composite. *J. Clin. Exp. Dent.* **9**, e945-951 (2017).
- 27. Adawi, H. et al. Effects of artificial aging of direct resin nano-hybrid composite on mean bond strength values for veneer ceramic samples. *Med. Sci. Monit.* **30**, e945243 (2024).
- 28. Almasabi, W. et al. Effect of water storage and thermocycling on light transmission properties, translucency and refractive index of nanofilled flowable composites. *Dent. Mater. J.* **40**, 599–605 (2021).
- 29. Hussin, R. et al. Vibrational studies of strontium antimony phosphate glass. Solid. State. Sci. Technol. 19, 363-370 (2011).
- Fu, S.-Y., Feng, X.-Q., Lauke, B. & Mai, Y.-W. Effects of particle size, particle/matrix interface adhesion and particle loading on mechanical properties of particulate-polymer composites. Compos. B. Eng. 39, 933-961 (2008).
- 31. Yokesh, C. A. et al. Comparative evaluation of the depth of cure and degree of conversion of two bulk fill flowable composites. *J. Clin. Diagn. Res.* 11(8), ZC86 (2017).
- 32. Morresi, A. L. et al. Thermal cycling for restorative materials: does a standardized protocol exist in laboratory testing? A literature review. *J. Mech. Behav. Biomed. Mater.* **29**, 295–308 (2014).
- Tian, J. et al. Multifunctional dental resin composite with antibacterial and remineralization properties containing nMgO-BAG. J. Mech. Behav. Biomed. Mater. 141, 105783 (2023).

Acknowledgements

This study was supported by the Korea Medical Device Development Fund grant funded by the Korea government (the Ministry of Science and ICT the Ministry of Trade, Industry and Energy, the Ministry of Health & Welfare, the Ministry of Food and Drug Safety) (Project Number: 2470000001, RS-2020-KD000261).

Author contributions

H.B.G., S.H.K., M.J.L., and J.S.K. conceived and designed the experiments. H.B.G., and S.H.K. performed all the experiments. H.B.G. and S.H.K. interpreted and analyzed the data. H.B.G. and S.H.K. conceived the study and wrote the manuscript. M.J.L. performed further experiments during the revision. J.S.K. provided manuscript writing assistance and critically revised the manuscript, adding important intellectual content. All authors reviewed and approved the final manuscript.

Funding

This research did not receive external funding.

Declarations

Competing interests

The authors declare no competing interests.

Additional information

Correspondence and requests for materials should be addressed to J.-S.K.

Reprints and permissions information is available at www.nature.com/reprints.

Publisher's note Springer Nature remains neutral with regard to jurisdictional claims in published maps and institutional affiliations.

Open Access This article is licensed under a Creative Commons Attribution-NonCommercial-NoDerivatives 4.0 International License, which permits any non-commercial use, sharing, distribution and reproduction in any medium or format, as long as you give appropriate credit to the original author(s) and the source, provide a link to the Creative Commons licence, and indicate if you modified the licensed material. You do not have permission under this licence to share adapted material derived from this article or parts of it. The images or other third party material in this article are included in the article's Creative Commons licence, unless indicated otherwise in a credit line to the material. If material is not included in the article's Creative Commons licence and your intended use is not permitted by statutory regulation or exceeds the permitted use, you will need to obtain permission directly from the copyright holder. To view a copy of this licence, visit http://creativecommons.org/licenses/by-nc-nd/4.0/.

© The Author(s) 2025